Desalination and Water Treatment
www.deswater.com

doi: 10.5004/dwt.2020.25635

189 (2020) 440–451
June

Preparation and characterization of cassava stem biochar for mixed reactive dyes removal from simulated effluent

Anand Navya[a], Sellakutti Nandhini[a], Selvaraju Sivamani[b,*], Gajendiran Vasu[b], Natesan Sivarajasekar[a], Ahmad Hosseini-Bandegharaei[c,d]

[a]*Department of Biotechnology, Kumaraguru College of Technology, Coimbatore, Tamil Nadu, India, Tel. +91 98940 24512; email: navyakct@gmail.com (A. Navya), Tel. +91 94429 83799; email: nandhinisapthavi@gmail.com (S. Nandhini), Tel. +91 95974 36327; email: sivarajasekar@gmail.com (N. Sivarajasekar)*
[b]*Chemical Engineering Section, Engineering Department, Salalah College of Technology, Salalah, Sultanate of Oman, Tel. +968 9069 4314; email: sivmansel@gmail.com (S. Sivamani), Tel. +968 9616 0879; email: gvasuchem@gmail.com (G. Vasu)*
[c]*Wastewater Division, Faculty of Health, Sabzevar University of Medical Sciences, Sabzevar, Iran, Tel. +98 93576 37687; email: ahoseinib@yahoo.com (A. Hosseini-Bandegharaei)*
[d]*Department of Engineering, Kashmar Branch, Islamic Azad University, Kashmar, Iran*

Received 27 August 2019; Accepted 6 February 2020

ABSTRACT

Treatment of the dyehouse effluent is essential to minimize the environmental pollution. Extensive literature is available on the adsorptive treatment of dyes using activated carbon prepared from low-value materials. But, the treatment of dyes using biochar provides two benefits: ease of biodegradability and use as a soil amendment. The main aim of the present study is to investigate the feasibility of the cassava stem biochar (CSB) for the removal of mixed reactive dyes from simulated effluent. Biochar was produced by slow pyrolysis under an argon atmosphere at 200°C–400°C at varying time and their yields were compared. In this work, batch trials were performed to study the adsorption of mixed reactive dyes [Reactive Red (RR) and Drimarene Turquoise (DT)] on CSB. The parameters examined for batch adsorption are pH, temperature, contact time, adsorbent dosage, initial dye concentration, and agitation speed. The maximum dye removal of 88.47% was found at an equilibrium time of 10 min and the optimum pH of 3. The mathematical models for isotherm, kinetics, and thermodynamics were analyzed to calculate maximum adsorption capacity, rate constant, and thermodynamic parameters, respectively. Adsorption followed Langmuir, Dubinin–Radushkevich (D–R) and Temkin isotherms. Pseudo-first-order model fitted well with the experimental data. Fourier transform infrared spectroscopy, scanning electron microscope, and X-ray diffraction of biochar were characterized before and after adsorption studies. Thus, the results showed that CSB could be utilized effectively for the removal of mixed reactive dyes from simulated effluent.

Keywords: Cassava stem; Biochar; Reactive dye; Pyrolysis; Adsorption

1. Introduction

The colors of life in full abundance are often exhibited through our attires. Dyes and dyestuff play an essential role in the coloring of fabrics [1]. Continuous usage and discharge of dyes along with the auxiliary chemicals, causes environmental degradation and ill effects for humans [2]. These dyes undergo phytochemical degradation in the water causing

* Corresponding author.

water pollution which is a menace to the life causing water-borne diseases such as cholera, typhoid, DNA damage, and finally death. Therefore, proper treatment of such water is mandatory before their release into the environment [3].

Inorganic pollutants like dyes and heavy metals are non-biodegradable and removed using unit operations such as coagulation and flocculation, sedimentation, flotation, membrane separation operations, and ion exchange [4]. Each unit operation has its merits and demerits, adsorption being the practically feasible method with minimum drawbacks. Adsorption is a surface phenomenon used for the removal of contaminants (adsorbate) from water using solid (adsorbent) [5,6]. Activated carbon, silica, alumina, bauxite, and clay are the commonly employed adsorbents [7,8]. Commercial activated carbon is widely used in process industries because of its high surface area. But, their use as adsorbent is limited due to high cost, low selectivity, and difficulty in the regeneration process. These shortfalls could be overcome by the use of cheap and natural materials as adsorbents mainly utilizing the agricultural and agro-industrial residues [9,10].

In the past decade, an alternative to the conventional adsorbents, biochar, a product of biomass pyrolysis, was also used as an adsorbent because of its effectiveness in the removal of impurities in water stream [11]. Biochar is obtained after the thermo-chemical conversion of biomass with limited or no oxygen under inert atmosphere [12]. Pyrolysis produces solid biochar (the main product of slow pyrolysis), liquid bio-oil (the main product of fast pyrolysis), or gaseous mixture (gasification product) [13]. Biochar with low adsorption capacity was produced at low temperature while biochar resulting from high temperature shows high adsorption capacity [14]. Hence, high temperature is favored by the thermal activation of biochar that increases adsorption capacity [15].

The materials used for biochar preparation are recycling coir pith [16], swede rape straw [17], *Acacia nilotica* leaves [18], sugarcane bagasse [19], teak tree bark powder [20], yellow passion fruit peel [21], cocoa shell [22], pistachio nut shells [23], neem bark and mango bark powder [24], anaerobic digestion residue, palm bark, and eucalyptus [25], bengal gram seed husk [26], wheat straw [27], corn straw [28], giant *Miscanthus* [29], municipal wastewater sludge [30], and cotton stalk [31].

Though cassava stem biochar (CSB) was employed for the removal of heavy metal ions [32], basic dyes [33,34] and atrazine [35], no studies were reported for the removal of reactive dyes. Thus, the study was emphasized on the adsorption of mixed reactive dyes from simulated effluent using CSB.

2. Materials and methods

2.1. Preparation of cassava stem biochar

Cassava stem of hybrid cultivar 740/92 was collected from Castor and Tapioca Research Station, Yethapur, Tamil Nadu, India. The stem was lopped to small pieces and dried in hot air oven (Narang Scientific Works Pvt. Ltd., New Delhi) to constant weight at 60°C. Then the dried sample was crushed to powder by using jaw crusher (Almech Enterprise, Coimbatore). The powder was then carbonized in chemical vapor deposition (CVD) chamber (VB ceramics consultants, Chennai) employing slow pyrolysis under an argon flow rate of 50 mL/min, and heating rate of 5°C/min to the desired temperature after which constant temperature was maintained. The resultant mixture was washed with double distilled water to remove ash and oil which leads to pure biochar. The biochar was then activated with 1% (w/v) oxalic acid solution in the solid to liquid ratio of 1:10 by placed in the incubated shaker (Scigenics Biotech Pvt. Ltd., Chennai) at 120 rpm and room temperature for 2 h. Then, the mixture was washed with double distilled water to remove excess acid, filtered using Whatman filter paper, and the precipitate was dried to constant weight in a hot air oven at 60°C. The final solid was used as CSB.

2.2. Preparation of simulated dye effluent

Reactive Red (RR) and Drimarene Turquoise (DT) were collected from the Common Effluent Treatment Plant, Arulpuram, Tamil Nadu, India. A simulated dye effluent was prepared in the laboratory by adding 1 g of RR and 1 g of DT in 1 L standard measuring flask and made up to the mark with tap water. The mixture was shaken well and warmed at 60°C to obtain a homogenous stock solution. Standard solutions were prepared from the stock solution. The maximum wavelength required for measuring dye concentration in the effluent was determined using UV-1800 UV-Visible Spectrophotometer [Shimadzu Analytical (India) Pvt. Ltd., Mumbai].

2.3. Batch adsorption studies

Batch adsorption studies were performed to evaluate the effect of pH, contact time, adsorbent dosage, temperature, agitation speed, and initial dye concentration on percentage dye removal and adsorption capacity by one-factor-at-a-time (OFAT) approach. In the OFAT approach, one factor was varied by maintaining all the other factors constant. The mathematical models for isotherm, kinetics, and thermodynamics were analyzed to calculate maximum adsorption capacity, rate constant and thermodynamic parameters, respectively. The outcomes of adsorption studies were adsorption capacity (q) and percentage dye removal (DR), calculated using Eqs. (1) and (2), respectively.

$$q = \frac{\left(C_i - C_0\right) \times V}{m} \left(\text{mg / g}\right) \tag{1}$$

$$\text{DR} = \frac{\left(C_i - C_0\right)}{C_i} \times 100 \left(\%\right) \tag{2}$$

where C_i is initial dye concentration, C_0 is final dye concentration, V is volume of solution, and m is mass of adsorbent.

2.3.1. Effect of pH

pH is one of the uncontrollable factors in the adsorption. So, it is essential to find optimum pH before varying any other factors. The effect of pH (2–7) was studied by maintaining

contact time of 15 min, agitation speed of 100 rpm, room temperature (27°C ± 5°C), initial dye concentration of 20 ppm and adsorbent dosage of 100 mg per 100 mL of a standard solution. A hundred milliliters of a standard solution of 20 ppm was mixed with 100 mg of biochar. The resultant mixture was filtered using Whatman filter paper, and the absorbance of the supernatant was measured in UV-visible spectrophotometer.

2.3.2. Effect of contact time

The effect of contact time was performed to study the adsorption kinetics and to calculate the equilibrium time of the adsorption. Equilibrium time is one of the critical factors in the design of adsorbers. The time was varied from 0 to 25 min by fixing pH at 3, initial dye concentration of 20 ppm, agitation speed of 100 rpm, adsorbent dosage of 100 mg per 100 mL of dye solution and at room temperature (27°C ± 5°C). After carried out the adsorption procedure, the mixture was filtered using Whatman filter paper, and the absorbance of the supernatant was measured in UV-visible spectrophotometer.

2.3.3. Effect of initial dye concentration

The effect of initial dye concentration was studied for adsorption isotherms, from which maximum adsorption capacity could be calculated. Isotherm studies were performed by varying initial dye concentration (4–100 ppm) by maintaining pH of 3, equilibrium time of 10 min, agitation speed of 100 rpm, adsorbent dosage of 100 mg per 100 mL of dye solution and room temperature (27°C ± 5°C). After carried out the adsorption procedure, the mixture was filtered using Whatman filter paper, and the absorbance of the supernatant was measured in UV-visible spectrophotometer.

2.3.4. Effect of temperature

The effect of temperature was performed to study the adsorption thermodynamics. The effect of temperature (25°C–45°C) was carried out by fixing pH of 3, time of 10 min, initial dye concentration of 20 ppm, agitation speed of 100 rpm, and adsorbent dosage of 100 mg per 100 mL of dye solution. After carried out the adsorption procedure, the mixture was filtered using Whatman filter paper, and the absorbance of the supernatant was measured in UV-visible spectrophotometer.

2.3.5. Effect of agitation speed

The effect of agitation speed was studied to enhance the mass transfer characteristics in adsorption. Agitation speed was varied from 50 to 150 rpm by fixing pH, time, initial dye concentration, temperature, and adsorbent dosage at 3, 10 min, 20 ppm, 27°C ± 5°C, and 200 mg per 100 mL of dye solution, respectively. After carried out the adsorption procedure, the mixture was filtered using Whatman filter paper, and the absorbance of the supernatant was measured in UV-visible spectrophotometer.

2.3.6. Effect of adsorbent dosage

The effect of adsorbent dosage was studied to effect the process economics. Excess usage of adsorbent increases the operational cost of the adsorption. Adsorbent dosage was varied from 50 mg to 400 mg per 100 mL of dye solution by maintaining pH at 3, time at 10 min, agitation speed at 100 rpm, initial dye concentration at 20 ppm, and room temperature at 27°C ± 5°C. After carried out the adsorption procedure, the mixture was filtered using Whatman filter paper, and the absorbance of the supernatant was measured in UV-visible spectrophotometer.

2.4. Characterization of adsorbent

CSB before and after adsorption was characterized for functional groups, surface morphology, and crystallinity using Fourier transform infrared spectroscopy (FTIR), scanning electron microscope (SEM), and X-ray diffraction (XRD), respectively.

2.4.1. Fourier transform infrared spectroscopy

The changes in functional groups before and after adsorption of mixed reactive dyes on CSB were investigated by ALPHA FTIR spectrophotometer (Bruker, USA). The FTIR spectrum was recorded in the wavenumber range from 4,000 to 400 cm^{-1}.

2.4.2. Scanning electron microscopey

SEM images of samples before and after adsorption were taken with an SEM (JSM 6390, JEOL, Japan). The surface morphology was examined with an accelerating voltage of 10 kV and a magnification of 1,500×.

2.4.3. X-ray diffraction

The crystallinity of the samples was evaluated by XRD (X'Pert PRO from PANalytical, the Netherlands) with a scanning rate of 5° per minute. The XRD patterns were obtained over the angular range $2\Delta = 10°–90°$.

3. Results and discussion

3.1. Maximum wavelength and calibration curve for the simulated dye effluent

Fig. 1 shows the UV-visible spectrum of simulated effluent. UV-visible spectrum was obtained by measuring absorbance against wavelength at a constant concentration. From Fig. 1, the maximum wavelength was found to be 540 nm. The Beer–Lambert law states that "The quantity of light absorbed by a substance dissolved in a fully transmitting solvent is directly proportional to the concentration of the substance and the path length of the light through the solution." The mathematical statement of the law is given in Eq. (3).

$$A = abc \tag{3}$$

where, A is the absorbance at maximum wavelength, a is the mass absorptivity, b is the path length, and c is the solute concentration. The calibration curve was plotted by measuring absorbance against the concentration of dye solution at constant path length and wavelength. Fig. 2 shows the linear calibration curve with mass absorptivity of 0.018 L/(mg cm) and determination coefficient R^2 of 0.994.

3.2. Optimization of pyrolysis of cassava stem for biochar production

Figs. 3a–c show the photographs of CSB at 200°C, 300°C, and 400°C at a constant time of 3 h after the pyrolysis of cassava stem for the production of biochar. It was found that at 200°C and 300°C, the sample was partially carbonized and at 400°C, cassava stem was completely carbonized. Figs. 3d–f show the photographs of CSB after 1, 2, and 3 h at 400°C. Cassava stem showed more carbonization at 3 h. Hence, 3 h and 400°C were found to be optimum time and temperature for the production of biochar from cassava stem.

3.3. Batch adsorption studies

3.3.1. Effect of pH

pH is the most influencing parameter in the adsorption process. Fig. 4a represents that the activated biochar from the cassava stem for the maximum removal efficiency (DR) was found to be 82.88% and the adsorption capacity (q) was obtained as 11.83 mg/g at the optimum pH 3. The cell walls of the cassava stem derived biochar has many functional groups on the surface. At this optimum pH, the biochar has more electrostatic attraction for dye effluent. There

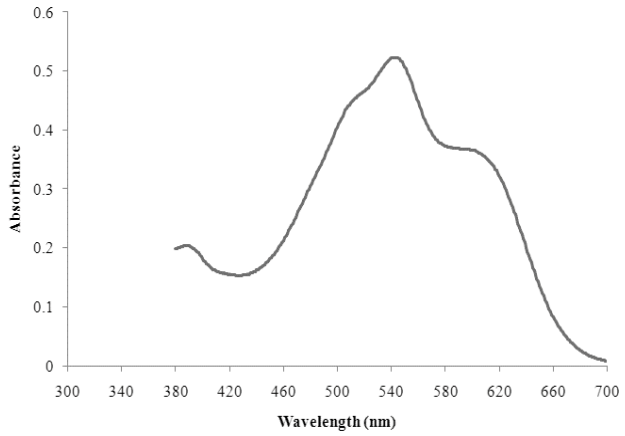

Fig. 1. UV-visible spectrum of simulated dye effluent.

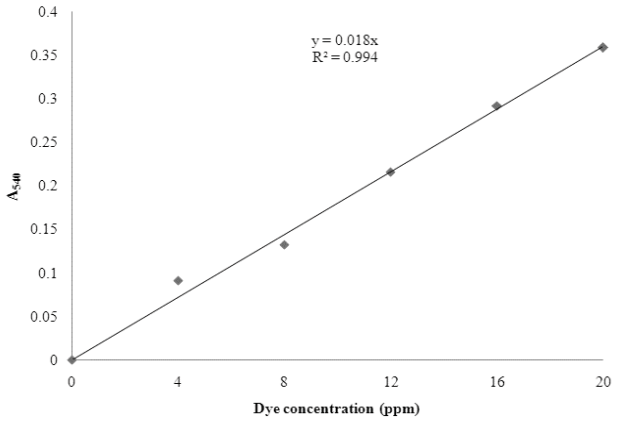

Fig. 2. Calibration curve for simulated dye effluent.

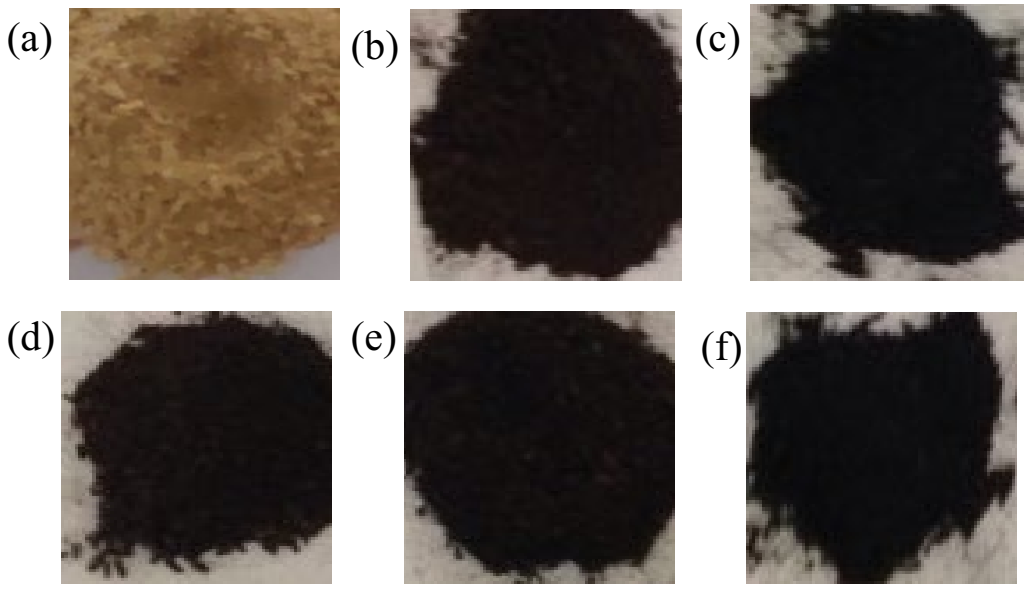

Fig. 3. Photographs of biochar at (a) 200°C, (b) 300°C, and (c) 400°C at constant time of 3 h, and after (d) 1 h, (e) 2 h, (f) 3 h at constant temperature of 400°C.

is a competition between the H^+ ions and the dye ions for the adsorption sites of adsorption leading to the inhibition of the dye adsorption. Zero-point charge (pH_{zpc}) is used to find whether the surface attains negative or positive charge as a function of the pH at which the net electric charge of the surface is zero. A pH value lower than the pH_{zpc} indicates that the superficial charge is positive and therefore, the adsorption of the anions is favored. For pH value higher than the pH_{zpc} shows that the superficial charge is negative and the adsorption of cations is favored. In the present study, pH is lesser than pH_{zpc}. The same pH was obtained as optimum for the removal of the light green dye using peanut husk as adsorbent [27]. Maximum adsorption of methylene blue using adsorbent raw barley straw at the pH of 11 [36]. The methylene blue adsorption was done with anaerobic digestion residue, palm bark, eucalyptus derived biochar at optimum pH 7 with maximum dye removal of 99.5%, 99.3%, and 86.1%, respectively, and adsorption capacity of 9.50 mg/g [25].

3.3.2. Effect of contact time

Fig. 4b shows that at pH 3, the contact time was perceived to be optimum at 10 min. The efficient removal was found to be 89.74%, and the adsorption capacity was 11.67 mg/g. Pesticide pymetrozine was effectively adsorbed at equilibrium time of 120 min with the brewers spent grain [13]. Acid black 172 was decolorized using bamboo biochar at the optimum time of 100 min [37].

3.3.3. Effect of initial dye concentration

The initial dye concentration influences the adsorption process. It was found that the maximum adsorption was observed at 20 ppm. Its efficient dye removal was attained at 78% and adsorption capacity at 15.47 mg/g, as illustrated in Fig. 4c. The effective removal of methylene blue was obtained for the initial dye concentration of about 200 mg/L using swede rape straw as adsorbate [17]. The maximum removal of malachite green dye was achieved by cashew nut shell with an optimum initial dye concentration of 20 mg/L [38].

3.3.4. Effect of temperature

The maximum dye removal was observed to about 88.47% and adsorption capacity of 18.33 mg/g at optimum temperature at 25°C as in Fig. 4d. Pesticide pymetrozine was removed with the help of brewers spent grain at 45°C [13]. About 83% of the congo red dye was removed by using nut shell as adsorbent [39]. When neem and mango bark were used as adsorbents, it was shown that the dye malachite green adsorbed well at 40°C [24].

3.3.5. Effect of agitation speed

At the optimum agitation speed of 100 rpm, the removal efficiency was found to be 79.27% and adsorption capacity to be 14.44 mg/g as in Fig. 4e. Teak tree bark powder was kept in contact with the methylene blue dye for about 30 min at the speed of 230 rpm due to which the dye was adsorbed well [20]. Lucrative removal of methyl violet 2B using *Casuarina equisetifolia* needle was achieved at 120 min and the optimum speed of 250 rpm [40].

3.3.6. Effect of adsorbent dosage

Fig. 4f explains that, at an optimum dosage of 100 mg per 100 mL of dye solution, it was shown that the maximum dye removal to be 79% and adsorption capacity of 13.92 mg/g. Yang et al. [37] achieved the adsorbent dosage to be 500 mg/L using bamboo biochar as an adsorbent for the adsorption of acid black 172. The methylene blue adsorption was done using anaerobic digestion residue, palm bark, eucalyptus biochar with the maximum adsorbent dosage of 5 mg/L which has a dye removal of 99.5%, 99.3%, and 86.1%, respectively [25]. At an optimum adsorbent dosage of 1 g/L, effective adsorption of copper and zinc ions took place with the help of hardwood and corn straw [41].

3.4. Adsorption kinetics

Adsorption kinetic studies are employed to assess the performance of the adsorbent. Pseudo-first-order (PFO), pseudo-second-order (PSO), Blanchard, Elovich, and intraparticle diffusion models were tested for the goodness of fit.

3.4.1. Pseudo first-order kinetics

The PFO is given by Eq. (4) as:

$$\ln\left(q_e - q_t\right) = \ln q_e - k_1 \times t \tag{4}$$

where q_e is the amount of dye adsorbed per unit mass of adsorbent at equilibrium time (mg/g), q_t is the amount of dye adsorbed per unit mass of adsorbent at any time t (mg/g), t is the contact time (min), and k_1 is the PFO rate constant. Fig. 5a was plotted between $\ln(q_e - q_t)$ and time to determine the values of q_e and k_1 from intercept and slope, respectively. The values of q_e and k_1 were found to be 13.57 mg/g and 0.198 min^{-1}, respectively. The R^2 value for this model was found to be 0.9195 which proved that the adsorption followed the PFO model.

3.4.2. Pseudo-second-order kinetics

The PSO kinetic model is given by Eq. (5) as:

$$\frac{t}{q_t} = \frac{1}{k_2 \times q_e^2} + \frac{t}{q_e} \tag{5}$$

where k_2 is the PSO rate constant. The graph between t/q_t along ordinate and time along abscissa gives the plot for the PSO kinetic model. q_e and k_2 can be determined from the intercept and the slope of the plot. From Fig. 5a, R^2 value of 0.6856 shows that the adsorption does not follow the PSO model.

3.4.3. Blanchard model

Blanchard postulated a second-order kinetic model which is given by Eq. (6) as:

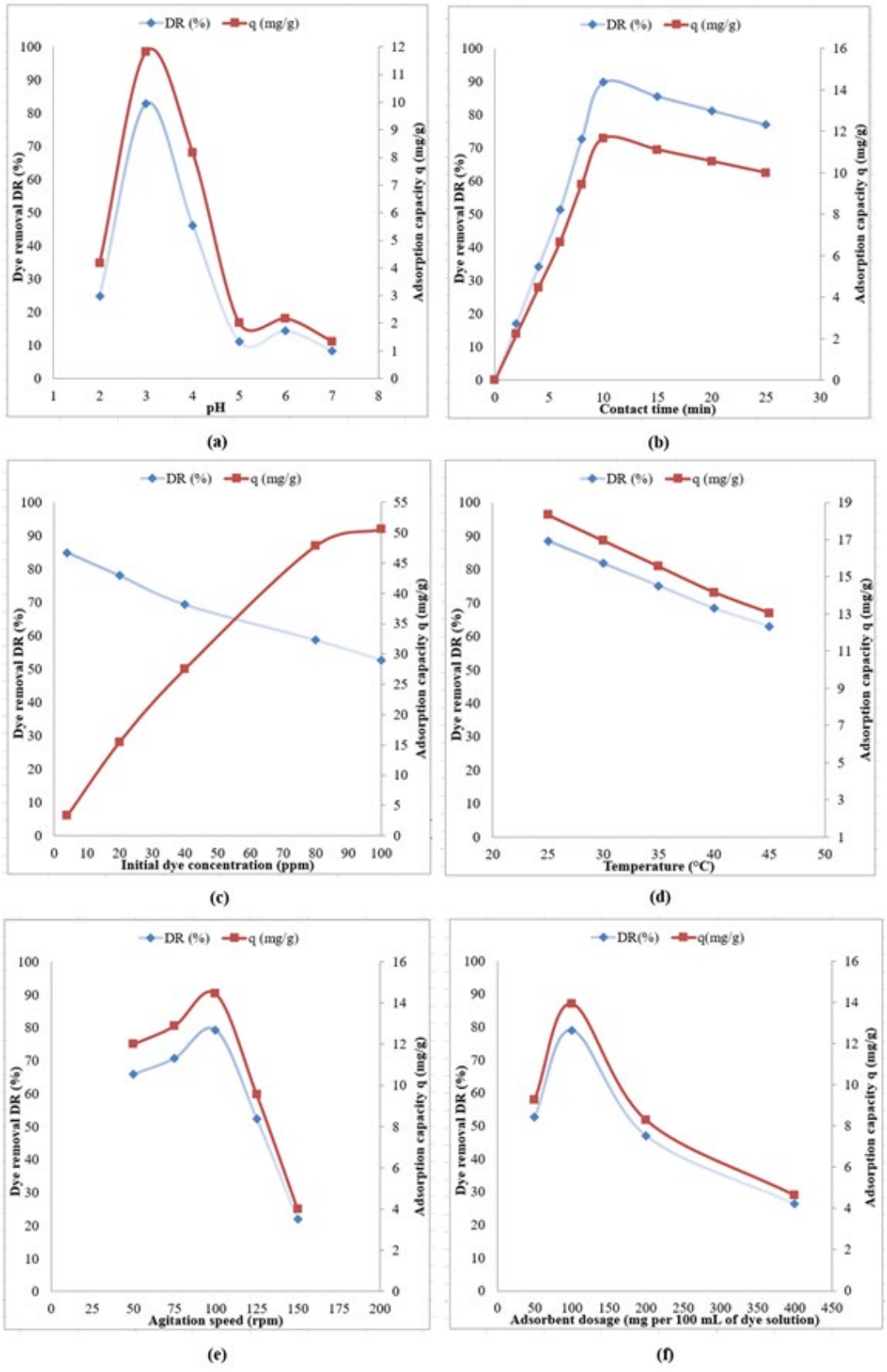

Fig. 4. Effect of (a) pH, (b) contact time, (c) initial dye concentration, (d) temperature, (e) agitation speed, and (f) adsorbent dosage on adsorption of simulated dye effluent on CSB.

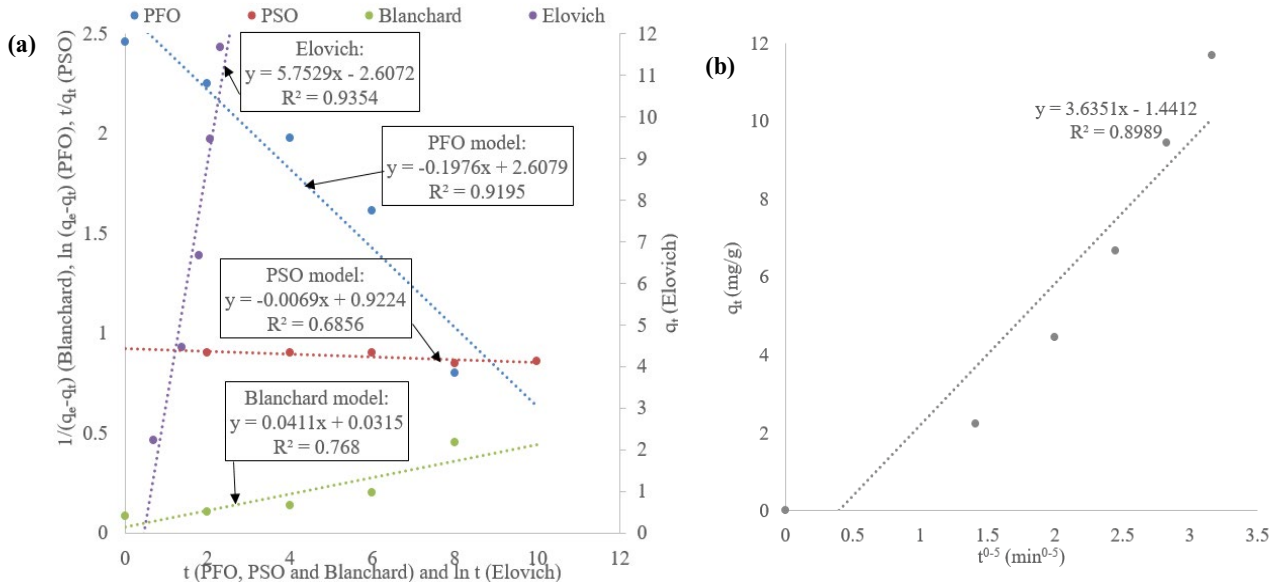

Fig. 5. Kinetic models using (a) pseudo-first-order (PFO), pseudo-second-order (PSO), Blanchard and Elovich equations and (b) intraparticle diffusion model on adsorption of simulated dye effluent on CSB.

$$\frac{1}{q_e - q_t} = k_b t + \gamma \tag{6}$$

where k_b is Blanchard rate constant and γ is the Blanchard model constant. Fig. 5a was plotted between $1/(q_e - q_t)$ and time to determine the values of k_b and γ from the slope and intercept, respectively. R^2 value of 0.768 shows that the adsorption does not follow the Blanchard second-order kinetic model.

3.4.4. Elovich model

Elovich postulated a second-order kinetic model assuming that the actual solid surfaces are heterogeneous. The model is given by Eq. (7) as:

$$q_t = \frac{1}{\beta}\ln(\alpha\beta) + \frac{1}{\beta}\ln(t) \tag{7}$$

where α is initial adsorption rate and β is the extent of surface coverage. The graph between q_t and time gives the plot for Elovich second-order kinetic model. α and β can be determined from the intercept and the slope of the plot, respectively, as 3.657 and 1.175 g/mg (Fig. 5a). The R^2 value for this model was found to be 0.9354, which proved that the adsorption followed the Elovich second-order model.

3.4.5. Intraparticle diffusion model

Intraparticle diffusion model is given by Eq. (8) as:

$$q_t = k_d t^{0.5} + C \tag{8}$$

where k_d is the rate constant, and C is the boundary layer thickness. The graph between q_t and $t^{0.5}$ gives the plot for the intraparticle diffusion model. C and k_d can be determined from the intercept and the slope of the plot. From Fig. 5b, it can be found that adsorption does not follow the intraparticle diffusion model because the value of intercept cannot be negative and R^2 is 0.8989.

3.5. Adsorption isotherms

To optimize the adsorber design, the isotherm model studies are carried out for the removal of the dye effluent with the biochar. The adsorption isotherm gives a better understanding of adsorption efficiency and characteristics of the mixed dye effluent on the surface of the biochar. The sorption characteristics were determined based on the coefficient of determination (R^2) emphasizes the strong affinity between adsorbent and the dye effluent.

3.5.1. Langmuir isotherm

Langmuir isotherm model is the adsorption model which is based on the homogenous surface. Langmuir isotherm model is given by Eq. (9) as:

$$\frac{1}{q_e} = \frac{1}{(q_m \times b)C_e} + \frac{1}{q_m} \tag{9}$$

where q_e is the amount of dye adsorbed per unit mass of adsorbent at equilibrium time (mg/g), C_e is the outlet dye concentration at equilibrium time (ppm), q_m is maximum adsorption capacity, and b is Langmuir constant. CSB is used for the decolourisation of the mixed reactive dye simulated effluent by adsorption which shows a linear plot by plotting $1/q_e$ as a function of $1/C_e$ with the regression value R^2 = 0.9986 (Fig. 6). So this model fits well with the data for all solutions, from diluted to concentrated solution.

Maximum adsorption capacity (q_m) for adsorption of simulated effluent on CSB was 49.75 mg/g and Langmuir constant was found to be 0.121 L/mg. Table 1 shows the maximum adsorption capacities for different adsorbates on adsorbents by Langmuir isotherm. The biochar derived from anaerobic digestion residue palm bark, eucalyptus for the removal of methylene blue dye has q_m of 9.77, 2.95, and 2 mg/g, respectively, following this model [25]. Thus, it was found that biochar from cassava stem has higher efficiency for the dye adsorption.

3.5.2. Freudlich isotherm

Freundlich isotherm model is the adsorption based on heterogeneous surface and the mathematical form is given by Eq. (10) as:

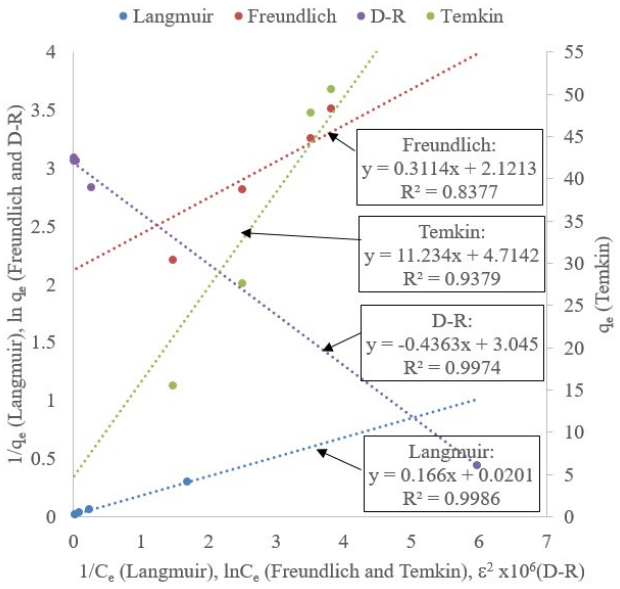

Fig. 6. Isotherm models using Langmuir, Freundlich, D-R and Temkin equations.

$$\ln q_e = \ln k_f + \left(\frac{1}{n}\right)\ln C_e \tag{10}$$

where, k_f and n are Freundlich constants. Freundlich isotherm is obtained by plotting $\ln q_e$ as a function of $\ln C_e$. From Fig. 6, R^2 value of 8377 shows that the adsorption does not follow the Freundlich isotherm.

3.5.3. Temkin isotherm

Temkin isotherm model is given by Eq. (11) as:

$$q_e = B\ln A + B\ln C_e \tag{11}$$

where A is Temkin isotherm binding constant at equilibrium (L/g), B is heat of adsorption constant = RT/b, b is Temkin constant (J/mol), R is universal gas constant (8.314 J/mol K), and T is temperature (K). The constants A, B and b, were found to be 1.521 L/g, 11.234 g/mg, and 220.54 J/mol, respectively, with R^2 value of 0.9379 (Fig. 6). Hence, adsorption of simulated effluent on CSB followed Temkin isotherm model. The constants of this isotherm were found to be b = 101 J/mol and A = 0.161 L/mg for the treatment of methylene blue dye using miswak leaves [42].

3.5.4. Dubinin–Radushkevich isotherm

The D–R isotherm model is given by Eq. (12) as:

$$\ln q_e = \ln q_m - k_{DR}\varepsilon^2 \tag{12}$$

$$\varepsilon = RT \times \ln\left(1 + \frac{1}{C_i}\right) \tag{13}$$

where k_{DR} is the adsorption energy constant, ε is the Polanyi potential and C_i is inlet dye concentration. In Fig. 6, a linear graph was obtained from the experimental data by plotting $\ln q_e$ as a function of ε^2. The constants were found to be k_{DR} = 0.4363 mol²/J² and q_m = 21.01 mg/g.

Table 1
Langmuir maximum adsorption capacity for different adsorbates on adsorbents

S. No	Biochar	Adsorbate	Langmuir maximum adsorption capacity q_m (mg/g)	References
1	Brewers spent grain	Pesticide Pymetrozine	31.606	[13]
2	*Miscanthus sacchariflorus*	Cadmium	13.24	[29]
3	(a) Activated cassava stem	Cadmium	(a) 24.88	[32]
	(b) Non-activated cassava stem	Cadmium	(b) 10.46	
4	Cellulosic municipal solid waste biochar	Azo dye	1.035	[38]
5	Hard wood	(i) Cu	(i) 6.79	[41]
		(ii) Zn	(ii) 4.54	
	Corn straw	(i) Cu	(i) 12.52	
		(ii) Zn	(ii) 11	
6	Cassava stem	Reactive dyes	Q = 49.75	Present study

Table 2
Functional groups for the corresponding wavenumber before and after adsorption of simulated effluent on CSB

Before adsorption		After adsorption	
Wavenumber (cm^{-1})	Functional groups	Wavenumber (cm^{-1})	Functional groups
3,371.57	N–H group	1,975.11	Aromatic combination bonds
2,931.80	Methylene C–H asym./sym.	1,897.95	Aromatic combination bonds
1,975.11	Aromatic combination bands	1,720.50	Aromatic combination bonds
1,921.10	Aromatic combination bands	1,581.63	C=C region
1,720.50	Aromatic combination bands	1,381.03	C–H region
1,381.03	*gem*-Dimethyl or ''iso''– (doublet)	1,319.31	C–N region
1,327.03	Skeletal C–C vibrations	1,172.72	C–O–C region
1,249.87	C–N group	1,033.72	Cyclohexane ring vibrations
1,041.56	Cyclohexane ring vibrations	964.41	Trans- C–H out of plane band
964.41	Skeletal C–C vibrations	810.10	1,4-disubstitution (para)
786.96	Skeletal C–C vibrations	763.81	Monosubstitution (phenyl)

3.6. Adsorption thermodynamics

Van't Hoff equation, proposed by Jacobus Henricus Van't Hoff, a Dutch chemist, has been utilized to find the changes in the state functions in a thermodynamic system. Van't Hoff equation is given by Eq. (14) as:

$$\ln K_c = \frac{-\Delta H^\circ}{RT} + \frac{\Delta S^\circ}{R} \tag{14}$$

where $K_c = \frac{(C_i - C_e)}{C_e}$ = equilibrium constant, C_i is inlet dye concentration, C_e is the outlet dye concentration at non-spontaneous equilibrium time, R is universal gas constant (8.314 J/mol K), T is temperature (K), ΔH° is the enthalpy of adsorption and ΔS° is the entropy of adsorption. Fig. 7 shows the plot of $\ln K_c$ as a function of (1/T). The enthalpy and entropy of adsorption were found to be –15.92 kJ/mol and –66.13 J/mol K, respectively. The negative value of the enthalpy signifies that the process is exothermic. The negative sign of entropy represents the reaction is non-spontaneous.

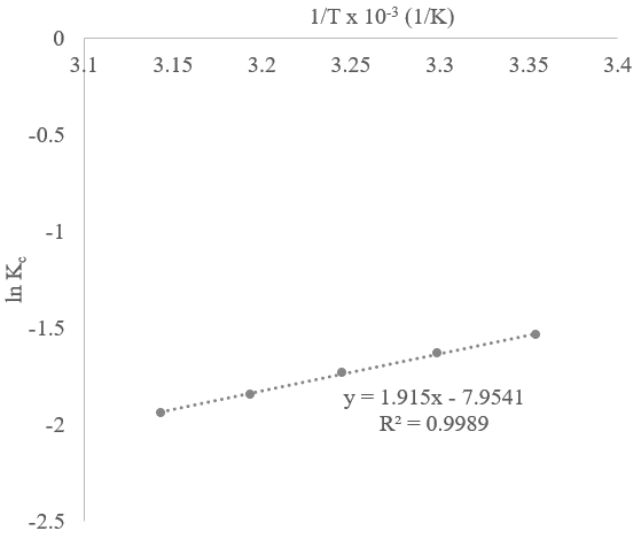

Fig. 7. Thermodynamic model using Van't Hoff equation on adsorption of simulated dye effluent on CSB.

3.7. Biochar characterization

3.7.1. Fourier transform infrared spectroscopy

Fig. 8 shows the presence of functional groups on the surface of the activated biochar in the range from 4,000 to 400 cm^{-1}. The functional groups were obtained at the specified wavenumbers before and after adsorption, as shown in Table 2. From the findings, it was reported that both biochar had varied functional groups that remained intact when adsorption occurs from dye effluent to CSB.

3.7.2. Scanning electron microscopey

The SEM was employed to examine the surface physical morphology of the CSB sample. From Fig. 9, it was seen that the fresh cassava stem derived biochar sample was flat in its

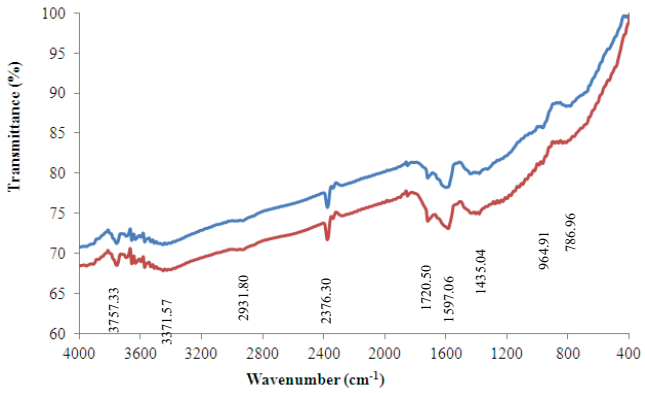

Fig. 8. FT-IR spectra of activated CSB before adsorption (blue line) and after adsorption (red line).

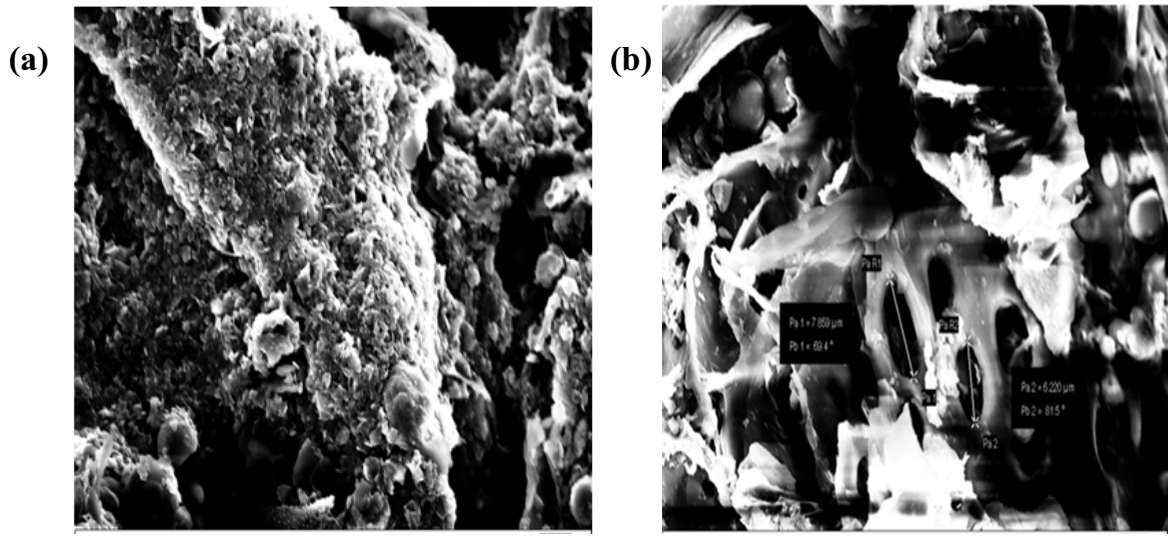

Fig. 9. SEM images of activated CSB (a) before adsorption and (b) after adsorption.

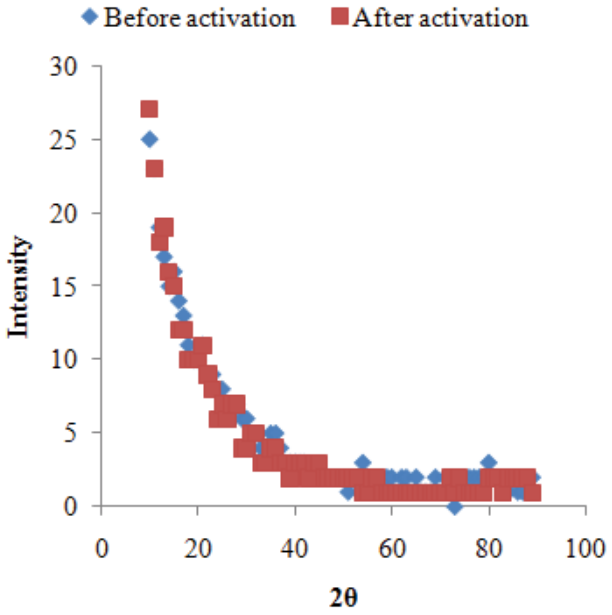

Fig. 10. XRD spectra of activated CSB before adsorption (blue line) and after adsorption (red line).

surface morphology without any pores. After adsorption, many pores were observed through which the adsorption of the dye has taken place.

3.7.3. X-ray diffraction

XRD technique is based on Bragg's equation. The constructive interferences and intensity peaks will be produced when incident X-rays affect the sample. The peak intensities detect the presence of a crystalline structure in the sample. But in Fig. 10, it confirms that CSB is completely amorphous and not crystalline.

4. Conclusion

In the present work, pyrolytic temperature and time were considered to be the significant factors that affect the biochar yield. The results revealed that the maximum biochar yield attained at 400°C for 3 h. pH, contact time, temperature, adsorbent dosage, and agitation speed were varied to study the batch adsorption studies of mixed reactive dye simulated effluent on CSB. The results exhibited the maximum dye removal at pH 3, time 10 min, temperature 25°C, adsorbent dosage of 100 mg per 100 mL of simulated effluent and agitation speed 100 rpm. Kinetic studies revealed that the adsorption followed PFO and Elovich second-order models and not followed PSO, Blanchard second order, and intraparticle diffusion models. Adsorption isotherm studies showed that the experimental data fitted well with Langmuir and Dubinin–Radushkevich (D–R) models with R^2 value > 0.99 and moderately with Temkin isotherm with R^2 value of 0.94 and not fitted with Freundlich isotherm. Thermodynamics revealed that the adsorption is exothermic and non-spontaneous. Characterization of adsorbents for functional groups using FTIR, surface morphology using SEM and crystallinity studies using XRD also favored the adsorption of simulated effluent on CSB. Thus, it is concluded that cassava stem derived biochar can be considered as the low-cost adsorbent for the decolorization of simulated dye effluent.

Acknowledgments

We would like to thank the faculty and staff of the Department of Nanotechnology, Sri Ramakrishna Engineering College, Coimbatore for providing necessary infrastructural facilities and support to carry out the work.

References

[1] S. Fan, Y. Wang, Z. Wang, J. Tang, J. Tang, X. Li, Removal of methylene blue from aqueous solution by sewage sludge-derived biochar: adsorption kinetics, equilibrium,

thermodynamics and mechanism, J. Environ. Chem. Eng., 5 (2017) 601–611.
[2] J.H. Li, G.H. Lv, W.B. Bai, Q. Liu, Y.C. Zhang, J.Q. Song, Modification and use of biochar from wheat straw (*Triticum aestivum* L.) for nitrate and phosphate removal from water, Desal. Water Treat., 57 (2016) 4681–4693.
[3] N. Zhu, T. Yan, J. Qiao, H. Cao, Adsorption of arsenic, phosphorus and chromium by bismuth impregnated biochar: adsorption mechanism and depleted adsorbent utilization, Chemosphere, 164 (2016) 32–40.
[4] S. Kizito, S. Wu, W.K. Kirui, M. Lei, Q. Lu, H. Bah, R. Dong, Evaluation of slow pyrolyzed wood and rice husks biochar for adsorption of ammonium nitrogen from piggery manure anaerobic digestate slurry, Sci. Total Environ., 505 (2015) 102–112.
[5] A. Bogusz, P. Oleszczuk, R. Dobrowolski, Application of laboratory prepared and commercially available biochars to adsorption of cadmium, copper and zinc ions from water, Bioresour. Technol., 196 (2015) 540–549.
[6] Y. Zhang, B. Cao, L. Zhao, L. Sun, Y. Gao, J. Li, F. Yang, Biochar-supported reduced graphene oxide composite for adsorption and coadsorption of atrazine and lead ions, Appl. Surf. Sci., 427 (2018) 147–155.
[7] S. Zhu, X. Huang, F. Ma, L. Wang, X. Duan, S. Wang, Catalytic removal of aqueous contaminants on N-doped graphitic biochars: inherent roles of adsorption and nonradical mechanisms, Environ. Sci. Technol., 52 (2018) 8649–8658.
[8] R. Khamirchi, A. Hosseini-Bandegharaei, A. Alahabadi, S. Sivamani, A. Rahmani-Sani, T. Shahryari, I. Anastopoulos, M. Miri, H.N. Tran, Adsorption property of Br-PADAP-impregnated multiwall carbon nanotubes towards uranium and its performance in the selective separation and determination of uranium in different environmental samples, Ecotoxicol. Environ. Saf., 150 (2018) 136–143.
[9] H. Bamdad, K. Hawboldt, S. MacQuarrie, A review on common adsorbents for acid gases removal: focus on biochar, Renewable Sustainable Energ. Rev., 81 (2018) 1705–1720.
[10] L. Chen, F. Li, Y. Wei, G. Li, K. Shen, H.J. He, High cadmium adsorption on nanoscale zero-valent iron coated *Eichhornia crassipes* biochar, Environ. Chem. Lett., 17 (2019) 589–594.
[11] N. Sivarajasekar, N. Mohanraj, S. Sivamani, J. Prakash Maran, I. Ganesh Moorthy, K. Balasubramani, Statistical optimization studies on adsorption of ibuprofen onto Albizialebbeck seed pods activated carbon prepared using microwave irradiation, Mater. Today:. Proc., 5 (2018) 7264–7274.
[12] D. Mohan, A. Sarswat, Y.S. Ok, C.U. Pittman Jr., Organic and inorganic contaminants removal from water with biochar, a renewable, low cost and sustainable adsorbent - a critical review, Bioresour. Technol., 160 (2014) 191–202.
[13] C. Parvathi, U.S. Shoba, C. Prakash, S. Sivamani, Manihot esculenta peel powder: effective adsorbent for removal of various textile dyes from aqueous solutions, J. Test. Eval., 46 (2018) 2299–2310.
[14] D. Kołodyńska, R. Wnętrzak, J.J. Leahy, M.H.B. Hayes, W. Kwapiński, Z. Hubicki, Kinetic and adsorptive characterization of biochar in metal ions removal, Chem. Eng. J., 197 (2012) 295–305.
[15] T. Clough, L. Condron, C. Kammann, C. Müller, A review of biochar and soil nitrogen dynamics, Agronomy, 3 (2013) 275–293.
[16] D. Kavitha, C. Namasivayam, Recycling coir pith, an agricultural solid waste, for the removal of procion orange from wastewater, Dyes Pigm., 74 (2007) 237–248.
[17] Y. Feng, H. Zhou, G. Liu, J. Qiao, J. Wang, H. Lu, C. Yang, Y. Wu, Methylene blue adsorption onto swede rape straw (*Brassica napus* L.) modified by tartaric acid: equilibrium, kinetic and adsorption mechanisms, Bioresour. Technol., 125 (2012) 138–144.
[18] T. Santhi, A.L. Prasad, S. Manonmani, A comparative study of microwave and chemically treated *Acacia nilotica* leaf as an eco friendly adsorbent for the removal of rhodamine B dye from aqueous solution, Arabian J. Chem., 7 (2014) 494–503.
[19] N. Sharma, B.K. Nandi, Utilization of sugarcane baggase, an agricultural waste to remove malachite green dye from aqueous solutions, J. Mater. Environ. Sci., 4 (2013) 1052–1065.
[20] S. Patil, S. Renukdas, N. Patel, Removal of methylene blue, a basic dye from aqueous solutions by adsorption using teak tree (*Tectona grandis*) bark powder, Int. J. Environ. Sci., 1 (2011) 711.
[21] F.A. Pavan, A.C. Mazzocato, Y. Gushikem, Removal of methylene blue dye from aqueous solutions by adsorption using yellow passion fruit peel as adsorbent, Bioresour. Technol., 99 (2008) 3162–3165.
[22] C. Theivarasu, S. Mylsamy, N. Sivakumar, Cocoa shell as adsorbent for the removal of methylene blue from aqueous solution: kinetic and equilibrium study, Universe J. Environ. Res. Technol., 1 (2011) 70–78.
[23] B. Armagan, F. Toprak, Optimum isotherm parameters for reactive azo dye onto pistachio nut shells: comparison of linear and non-linear methods, Pol. J. Environ. Stud., 22 (2013) 1007–1011.
[24] R. Srivastava, D.C. Rupainwar, A comparative evaluation for adsorption of dye on neem bark and mango bark powder, Indian J. Chem. Technol., 18 (2011) 67–75.
[25] L. Sun, S. Wan, W. Luo, Biochars prepared from anaerobic digestion residue, palm bark, and eucalyptus for adsorption of cationic methylene blue dye: characterization, equilibrium, and kinetic studies, Bioresour. Technol., 140 (2013) 406–413.
[26] M.S. Reddy, V. Nirmala, C. Ashwini, Bengal gram seed husk as an adsorbent for the removal of dye from aqueous solutions–batch studies, Arabian J. Chem., 10 (2017) S2554–S2566.
[27] Y. Su, B. Zhao, W. Xiao, R. Han, Adsorption behavior of light green anionic dye using cationic surfactant-modified wheat straw in batch and column mode, Environ. Sci. Pollut. Res., 20 (2013) 5558–5568.
[28] C. Umpuch, B. Jutarat, Adsorption of organic dyes from aqueous solution by surfactant modified corn straw, Int. J. Chem. Eng. Appl., 4 (2013) 134.
[29] W.K. Kim, T. Shim, Y.S. Kim, S. Hyun, C. Ryu, Y.K. Park, J. Jung, Characterization of cadmium removal from aqueous solution by biochar produced from a giant *Miscanthus* at different pyrolytic temperatures, Bioresour. Technol., 138 (2013) 266–270.
[30] W. Zhang, S. Mao, H. Chen, L. Huang, R. Qiu, Pb(II) and Cr(VI) sorption by biochars pyrolyzed from the municipal wastewater sludge under different heating conditions, Bioresour. Technol., 147 (2013) 545–552.
[31] J. Ren, N. Li, L. Li, J.K. An, L. Zhao, N.Q. Ren, Granulation and ferric oxides loading enable biochar derived from cotton stalk to remove phosphate from water, Bioresour. Technol., 178 (2015) 119–125.
[32] S. Prapagdee, S. Piyatiratitivorakul, A. Petsom, Activation of cassava stem biochar by physico-chemical method for stimulating cadmium removal efficiency from aqueous solution, *Environment Asia*, 7 (2014) 60–69.
[33] L. Meili, R.P.S. Godoy, J.I. Soletti, S.H.V. Carvalho, L.M.O. Ribeiro, M.G.C. Silva, M.G.A. Vieira, M.L. Gimenes, Cassava (*Manihot esculenta* Crantz) stump biochar: physical/chemical characteristics and dye affinity, Chem. Eng. Commun., 206 (2019) 829–841.
[34] M.K.Z.M. Zaid, N.A. Jamion, Q. Omar, S.K. Yong, Sorption of malachite green (MG) by cassava stem biochar (CSB) kinetic and isotherm studies, J. Fundam. Appl. Sci., 9 (2017) 273–287.
[35] J. Luo, C. Ge, H. Yu, D. Feng, P. Huang, F. Li, Cassava waste derived biochar as soil amendments: effects on kinetics, equilibrium and thermodynamics of atrazine adsorption, Fresenius Environ. Bull., 25 (2016) 4607–4617.
[36] J. Yu, X. Zhang, D. Wang, P. Li, Adsorption of methyl orange dye onto biochar adsorbent prepared from chicken manure, Water Sci. Technol., 77 (2018) 1303–1312.
[37] Y. Yang, X. Lin, B. Wei, Y. Zhao, J. Wang, Evaluation of adsorption potential of bamboo biochar for metal-complex dye: equilibrium, kinetics and artificial neural network modelling, Int. J. Environ. Sci. Technol., 11 (2014) 1093–1100.
[38] M. Agarwal, J. Tardio, S.V. Mohan, Pyrolysis biochar from cellulosic municipal solid waste as adsorbent for azo dye

removal: equilibrium isotherms and kinetics analysis, Int. J. Environ. Sci. Dev., 6 (2015) 67–72.
[39] F. Papari, P.R. Najafabadi, B. Ramavandi, Fluoride ion removal from aqueous solution, groundwater, and seawater by granular and powdered *Conocarpus erectus* biochar, Desal. Water Treat., 65 (2017) 375–386.
[40] D. Angın, E. Altintig, T.E. Köse, Influence of process parameters on the surface and chemical properties of activated carbon obtained from biochar by chemical activation, Bioresour. Technol., 148 (2013) 542–549.
[41] X. Chen, G. Chen, L. Chen, Y. Chen, J. Lehmann, M.B. McBride, A.G. Hay, Adsorption of copper and zinc by biochars produced from pyrolysis of hardwood and corn straw in aqueous solution, Bioresour. Technol., 102 (2011) 8877–8884.
[42] M. Inyang, B. Gao, Y. Yao, Y. Xue, A.R. Zimmerman, P. Pullammanappallil, X. Cao, Removal of heavy metals from aqueous solution by biochars derived from anaerobically digested biomass, Bioresour. Technol., 110 (2012) 50–56.